Author(s): Almosly, Wafa; Carlsson, B. G.; Dobaczewski, Jacek; Suhonen, Jouni; Toivanen, Jussi; Vesely, P.; Ydrefors, Emanuel

Title: Charged-current neutrino and antineutrino scattering off 116Cd described by Skyrme forces

Year: 2014

Version:

Please cite the original version:

Almosly, W., Carlsson, B. G., Dobaczewski, J., Suhonen, J., Toivanen, J., Vesely, P., & Ydrefors, E. (2014). Charged-current neutrino and antineutrino scattering off 116Cd described by Skyrme forces. Physical Review C, 89(2), Article 024308. https://doi.org/10.1103/PhysRevC.89.024308

Charged-current neutrino and antineutrino scattering off ^{116}Cd described by Skyrme forces

W. Almosly,[1] B. G. Carlsson,[2] J. Dobaczewski,[1] J. Suhonen,[1] J. Toivanen,[1] P. Vesely,[3,4] and E. Ydrefors[1,5]

[1]*Department of Physics, University of Jyväskylä, P.O. Box 35 (YFL), FI-40114 Jyväskylä, Finland*

[2]*Division of Mathematical Physics, LTH, Lund University, P.O. Box 118, S-22100 Lund, Sweden*

[3]*Nuclear Physics Institute, 25068 Rez, Czech Republic*

[4]*Faculty of Mathematics and Physics, Charles University in Prague, Prague, Czech Republic*

[5]*Royal Institute of Technology (KTH), Alba Nova University Center, SE-10691 Stockholm, Sweden*

(Received 8 November 2013; revised manuscript received 15 January 2014; published 13 February 2014)

We perform calculations of the cross sections for charged-current neutrino and antineutrino scattering off ^{116}Cd using ten different Skyrme interactions, at energies typical of supernova neutrinos. We use the quasiparticle random-phase approximation in its charged-changing mode (pnQRPA) to construct the required nuclear wave functions for the participant initial and final states. We compare the results of these calculations with the results of calculations based on the Bonn one-boson-exchange potential. The response of ^{116}Cd to supernova neutrinos is calculated by folding the obtained cross sections with suitably parametrized Fermi-Dirac distributions of the electron-neutrino and electron-antineutrino energies.

DOI: 10.1103/PhysRevC.89.024308 PACS number(s): 21.60.Jz, 25.30.Pt, 27.60.+j, 21.30.−x

I. INTRODUCTION

Studies of the neutrino and its properties constitute one of the most important subjects in modern nuclear/particle physics. Open questions which still remain unanswered are, e.g., the Dirac-or-Majorana nature of the neutrino, if the mass hierarchy is normal or inverted, and the absolute values of the neutrino masses. Recently, it has also been confirmed that the value of the third neutrino mixing angle, θ_{13}, has a rather large value of $\sin^2\theta_{13} = 0.025$ [1]. This opens up the possibility of future large-scale detectors to determine the value of the currently unknown CP violation phase [2].

Neutrinoless double-beta decay of a suitable nucleus, if it exists, would be a potential method to measure the absolute neutrino mass (see, e.g., [3]). A detection of neutrinoless double-beta decay would also provide direct evidence whether the neutrino is a Majorana particle. One presently running experiment for such studies is the COBRA [4] which is based on ^{116}Cd. Nuclear-structure studies of this nucleus and its beta-decay partners ^{116}In and ^{116}Ag are therefore of great interest.

Neutrinos from supernovae carry important information both concerning the details of the supernova dynamics and nucleosynthesis of heavy elements. Neutrinos from either man-made sources or from astrophysical ones (the Sun, supernovae, etc.) can be detected by using charged-current and/or neutral-current neutrino scatterings off nuclei [5,6]. Charged-current neutrino-nucleus scattering could in the future be used to constrain the theoretical predictions of nuclear matrix elements for neutrinoless double-beta decay by exploiting neutrino beams, e.g., so-called beta beams [7].

Neutrinos from supernovae have energies of a few tens of MeV up to about 100 MeV. Consequently, transitions to states in the final nucleus with excitation energies of 10–20 MeV or even more could be important. However, knowledge about the high-energy part of the excitation energy spectrum of the final nucleus is typically quite limited, apart from some gross information on giant resonances. It is therefore important to perform calculations of neutrino-nucleus cross sections based on different theoretical approaches. The nuclear energy-density functional theory has been shown to be able to successfully describe bulk properties of many medium-heavy and heavy nuclei [8]. In such calculations global two-body interactions are adopted and they are thus well suited for systematic studies of neutrino-nucleus cross sections which are of interest for supernova simulations and studies of nucleosynthesis of heavy elements. It is also interesting to test the ability of globally adjusted two-body interactions (like Skyrme interactions) to describe weak-interaction processes which are sensitive to the details of nuclear structure (e.g., neutrino-nucleus cross sections). Global features of the nuclear methods are important in order to estimate the neutrino-nucleus cross sections for nuclei for which the experimental data is very limited (e.g., for nuclei far from stability).

In our previous works (see, e.g., [9,10]) we have computed the cross sections for the charged-current and neutral-current neutrino nucleus scatterings off the stable molybdenum isotopes. These calculations were based on the Bonn one-boson-exchange potential [11] and the parameters of the Hamiltonian were adjusted locally, i.e., to the nucleus under consideration. The same line of work was later extended to the study of ^{116}Cd [12]. In this paper we extend our studies of ^{116}Cd and perform self-consistent calculations of the cross sections for the charged-current neutrino and antineutrino scatterings off ^{116}Cd based on ten different globally parametrized Skyrme interactions; see Ref. [13] for references to papers defining older parametrizations and Ref. [14] for the recent UDF1 parametrization. We compare the Skyrme results with those obtained by using the locally adjusted Bonn potential. In the Skyrme-based computations a large valence space consisting of 15 main harmonic oscillator shells is adopted. In order to make such large-scale calculations feasible we employ in the present work the method introduced in Refs. [9,10] for the computations of the needed nuclear matrix elements. The Gamow-Teller strengths computed with the Bonn and different Skyrme interactions are compared with each other and with experimental data. The nuclear response to supernova

TABLE I. The values of the pairing strength G_1 used in this work for each Skyrme interaction type. The third column gives the ratio of the critical value of the parameter G_0 to G_1 for the values of G_1 displayed in column 2. The critical value refers to the value where the pnQRPA calculation breaks down. Also are given the size of the proton $Z = 50$ energy gap, the spin-parity of the calculated odd-odd ground state, and the excitation energy of the first 1^+ state.

Skyrme type	G_1 (MeV fm^3)	G_0(crit)/G_1	$Z = 50$ energy gap	J^π of the ground state	$E(1_1^+)$ (MeV)
SkX	(−560, −600)	(−18.04, −17.17)	5.447	4^+	0.21–0.27
SkM*	(−605, −667)	(−19.17, −17.47)	5.678	4^+	0.056-0.083
SkP	(−557, −609)	(−17.41, −16.75)	4.174	4^+	0.024–0.050
UDF0	(−542, −573)	(−17.34, −17.28)	4.395	4^+	0.039–0.065
UDF1	(−567, −599)	(−17.46, −16.69)	4.908	3^+	0.11–0.14
SIII	(−608, −666)	(−18.75, −17.42)	6.270	4^+	0.47–0.63
SV	(−883, −901)	(−30.58, −22.20)	8.274	4^+	2.66–2.73
SLy5	(−665, −693)	(−18.50, −18.18)	5.639	4^+	0.18–0.20
SLy4	(−680, −693)	(−18.09, −18.18)	5.809	4^+	0.27–0.29
SLy4d	(−687, −701)	(−19.36, −19.12)	6.523	4^+	0.62–0.66

neutrinos is subsequently estimated by folding the obtained cross sections with suitably parametrized Fermi-Dirac distributions of the electron-neutrino and electron-antineutrino energies.

This paper is organized as follows. In Sec. II the formalism for the Skyrme-based pnQRPA calculations is briefly summarized. Then, in Sec. III the formalism for the charged-current neutrino scattering is briefly discussed. In Sec. IV we present our results and finally, in Sec. V, we draw the conclusions.

II. QUASIPARTICLE RANDOM-PHASE APPROXIMATION USING A SKYRME FORCE

A. HFB equation for even-even ground states

The pnQRPA calculations with Skyrme interaction were based on a spherical Hartree-Fock-Bogoliubov (HFB) ground state. The code HOSPHE [15,16] was used to calculate both the HFB ground state and the pnQRPA excitations. HOSPHE calculates solutions to the spherical HFB equations

$$\begin{pmatrix} h-\lambda I & \Delta \\ \Delta^+ & -h^*+\lambda I \end{pmatrix}\begin{pmatrix} U & V^* \\ V & U^* \end{pmatrix} = \begin{pmatrix} U & V^* \\ V & U^* \end{pmatrix}\begin{pmatrix} E & 0 \\ 0 & -E \end{pmatrix}, \tag{1}$$

which define the quasiparticle operators through the Bogoliubov-Valatin transformation

$$\alpha^\dagger_{kljm} := \sum_n \left(U^{lj}_{kn} a^\dagger_{nljm} + V^{lj}_{kn} a_{nljm}\right). \tag{2}$$

The Skyrme interactions used in this work are density-dependent two-body interactions. Therefore the matrices h in the HFB equations, and the HFB ground-state energy expression contain rearrangement terms that take this density dependence into account. A finite range, nonlocal, separable, Gaussian pairing interaction

$$V(\mathbf{r}_1,\mathbf{r}_2,\mathbf{r}'_1,\mathbf{r}'_2) = \delta(\mathbf{R}-\mathbf{R}')P(r)P(r')[G_0\widehat{\Pi}_{s=0} + G_1\widehat{\Pi}_{s=1,T=0}], \tag{3}$$

where

$$\widehat{\Pi}_{s=0} = \tfrac{1}{2}(1-\widehat{P}_\sigma), \quad \widehat{\Pi}_{s=1,T=0} = \tfrac{1}{4}(1+\widehat{P}_\sigma)(1-\widehat{P}_\tau) \tag{4}$$

was used for the pairing matrices Δ of the HFB equation. The normalized radial function is defined as

$$P(r) = \frac{1}{(4\pi a^2)^{3/2}} e^{-\frac{r^2}{4a^2}}, \tag{5}$$

and the parameter a determines the range of the interaction. This particle-particle interaction does not have density dependence, and because of its finite range no pairing cutoff regularization is needed. The G_1 pairing strength and the interaction range a were determined by a global fit to the experimental pairing gaps of semimagic isotopic chains in Ref. [17]. Therefore the pairing strength and range depend only on the used Skyrme interaction. A range parameter $a = 0.660$ fm was used in Refs. [17,18] for the Skyrme interactions SkX, SLy4, and SkM* and the same range is adopted here for the other Skyrme forces.

TABLE II. Experimetal and computed centroids of the major and minor satellites of the Gamow-Teller giant resonance in ^{116}In. The energies are given relative to the ground state of ^{116}In.

	Exp	Bonn	SkX	SkM*	SkP	SIII
Centroid of GTGR$_1$ (MeV)	14.5 [24]	14.6	12.15–12.58	15.74–16.34	11.41–11.88	15.33–15.91
Centroid of GTGR$_2$ (MeV)	8.9 [24]	7.3	6.29–6.82	8.04–8.65	4.87–5.43	8.87–9.43

UDF0	UDF1	SV	SLy5	SLy4	SLy4d
12.79-13.17	12.47–12.86	22.09–22.33	13.92–14.21	15.58–15.67	16.32–16.47
6.0-6.4	5.86–6.09	13.1–13.4	6.14–6.41	8.59–8.68	9.03–9.19

TABLE III. Experimental and computed Gamow-Teller sum strengths for the major and minor Gamow-Teller satellites in ^{116}In (first two lines). The third line gives the transition strength to the ground state.

	Σ_{exp}	Σ_{Bonn}	Σ_{SkX}	$\Sigma_{\text{SkM*}}$	Σ_{SkP}
GTGR_1	25.8 ± 4.1 [24]	27.3	21.35–21.90	22.13–23.62	15.89–16.90
GTGR_2	6.6 ± 1.1 [24]	7.5	18.91–20.15	16.71–17.01	29.57–29.73
g.s.	0.65 ± 0.12 (stat.) ± 0.10 (syst.) [25]	1.8	1.66–1.74	0.84–0.90	1.74–2.11

Σ_{UDF0}	Σ_{UDF1}	Σ_{SIII}	Σ_{SV}	Σ_{SLy5}	Σ_{SLy4}	Σ_{SLy4d}
23.57–23.85	24.06–24.57	24.99–25.01	18.59–19.08	13.04–13.73	22.81–23.02	22.99–23.44
15.38–15.80	12.60–14.08	10.97–11.49	16.66–17.67	32.93–32.96	15.30–15.98	16.26–16.27
0.85–0.88	0.77–0.78	1.27–1.28	1.346–1.354	2.94–3.08	1.171–1.174	1.252–1.253

B. pnQRPA equations

The pnQRPA equations were solved using the full diagonalization method implemented in the code HOSPHE. The proton-neutron particle-hole residual interaction is derived from the same Skyrme interaction as was used in the HFB calculation. The pairing interaction used in the pnQRPA calculations is also the same as used in the HFB calculation for the ground state, except for the $T = 0$ pairing channel which is not active in the HFB calculation. The $T = 0$ part of the pairing interaction does not contribute to the energies of double-even nuclei, if proton-neutron mixing is not present in the HFB ground state. Therefore this pairing strength must be fitted separately, using experimental data about odd-odd nuclei. Fits of G_0 show that a good choice is $G_0 \approx G_1$ [19].

Because the $T = 0$ pairing interaction does not contribute to the HFB state, a too large value for G_0 strength can cause the pnQRPA to collapse and give unphysical zero energy solutions.

III. CHARGED-CURRENT NEUTRINO-NUCLEUS SCATTERING

In this work we consider charged-current neutrino or antineutrino scatterings off an even-even nucleus (A, Z) with mass number A and proton number Z. The formalism for the calculation of neutrino-nucleus cross sections have already been reviewed many times in the literature; see, e.g., Refs. [20–22]. Therefore, in this section we only give a brief summary of the theory. For more details we refer to the aforementioned references.

In the present computations the impinging neutrino has an energy of $E \lesssim 100$ MeV. Thus, the transferred momentum $Q^2 = -q_\mu q^\mu \ll M_W^2$, where M_{W} is the mass of the charged boson. In this energy range the weak-interaction vertex can be described as pointlike and the matrix element of the effective Hamiltonian can then be written in the form

$$\langle f|H_{\text{eff}}|i\rangle = \frac{G}{\sqrt{2}} \int d^3\mathbf{r} l_\mu e^{-i\mathbf{q}\cdot\mathbf{r}} \langle f|\mathcal{J}^\mu(\mathbf{r})|i\rangle, \tag{6}$$

where l_μ is the lepton matrix element (see, e.g., [9]) and $\mathcal{J}^\mu(\mathbf{r})$ denotes the nuclear current. In this work we assume that the final and initial states have good angular momenta J_f and J_i and parities π_f and π_i. In order to take advantage of this one performs a multipole expansion of the matrix element by using the plane-wave expansion

$$e^{i\mathbf{q}\cdot\mathbf{r}} = \sum_l i^l \sqrt{4\pi(2l+1)} j_l(qr) Y_{l0}(\theta_r, \phi_r), \tag{7}$$

where $q = |\mathbf{q}|$ and $r = |\mathbf{r}|$.

The total cross section for the charged-current (anti)neutrino scattering of a nucleus as a function of the energy $E_{\mathbf{k}}$ of the impinging neutrino (or antineutrino) can then be written in the form

$$\sigma(E_{\mathbf{k}}) = \sum_f \int \sin\theta \, d\theta \left[\frac{d\sigma}{d\theta}\right]_{i\to f}, \tag{8}$$

where the sum is over all included final nuclear states and θ is the angle between the incoming and outgoing leptons. In Eq. (8) the differential cross section is given by

$$\left[\frac{d\sigma}{d\theta}\right]_{i\to f} = \frac{2G^2|\mathbf{k}'|E_{\mathbf{k}'}}{(2J_i+1)} F(\pm Z_f, E_{\mathbf{k}'}) \left(\sum_{J\geq 0} \sigma_{\text{CL}}^J + \sum_{J\geq 1} \sigma_{\text{T}}^J\right), \tag{9}$$

where

$$\begin{aligned}\sigma_{\text{CL}}^J &= (1 + a\cos\theta)|(J_f\|\mathcal{M}_J(q)\|J_i)|^2 \\ &\quad + (1 + a\cos\theta - 2b\sin^2\theta)|(J_f\|\mathcal{L}_J(q)\|J_i))|^2 \\ &\quad + \frac{E_{\mathbf{k}} - E_{\mathbf{k}'}}{q}(1 + a\cos\theta) + c) \\ &\quad \times 2\text{Re}[(J_f\|\mathcal{L}_J(q)\|J_i)(J_f\|\mathcal{M}_J(q)\|J_i)^*],\end{aligned} \tag{10}$$

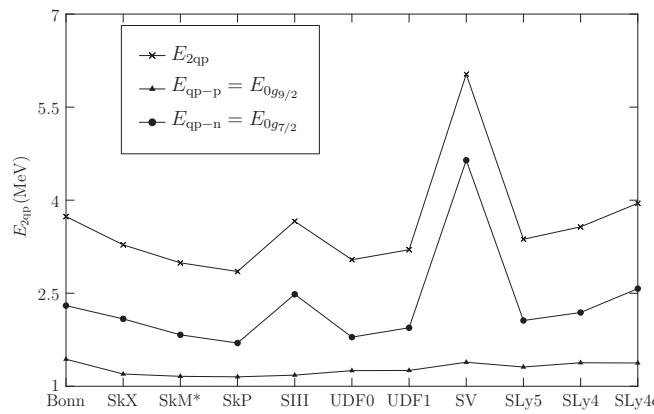

FIG. 1. The proton-$0g_{9/2}$ and the neutron-$0g_{7/2}$ quasiparticle energies, and the sum of these energies, for all the Skyrme interactions and the Bonn interaction.

and

$$\sigma_{\mathrm{T}}^{J} = (1 - a\cos\theta + b\sin^2\theta) \times \left[\left|\left(J_f\left\|\mathcal{T}_J^{\mathrm{mag}}(q)\right\|J_i\right)\right|^2 + \left|\left(J_f\left\|\mathcal{T}_J^{\mathrm{el}}(q)\right\|J_i\right)\right|^2\right] \mp \frac{(E_{\mathbf{k}} + E_{\mathbf{k}'})}{q}[(1 - a\cos\theta) - c)] \times 2\mathrm{Re}\left[\left(J_f\left\|\mathcal{T}_J^{\mathrm{mag}}(q)\right\|J_i\right)\left(J_f\left\|\mathcal{T}_J^{\mathrm{el}}(q)\right\|J_i\right)^*\right]. \quad (11)$$

In the expressions above $\mathbf{k}'$ is the three-momentum and $E_{\mathbf{k}'}$ is the energy of the outgoing electron or positron. For more details we refer to Ref. [9].

The operators $\mathcal{T}_{JM} = \mathcal{M}_{JM}, \mathcal{L}_{JM}, \mathcal{T}^{\mathrm{el}}_{JM}, \mathcal{T}^{\mathrm{mag}}_{JM}$ contain in general both vector and axial-vector pieces, i.e., $\mathcal{T}_{JM} = T^{\mathrm{V}}_{JM} - T^{\mathrm{A}}_{JM}$. Here, the operators M^{V}_{JM}, L^{V}_{JM}, $T^{\mathrm{el,V}}_{JM}$, and $T^{\mathrm{mag,A}}_{JM}$ have parity $(-1)^J$ and the rest of the operators have parity $(-1)^{J+1}$. Consequently, 0^+ transitions are of purely vector type. Similarly, transitions mediated by the 0^- multipole are of axial-vector character. However, for transitions mediated

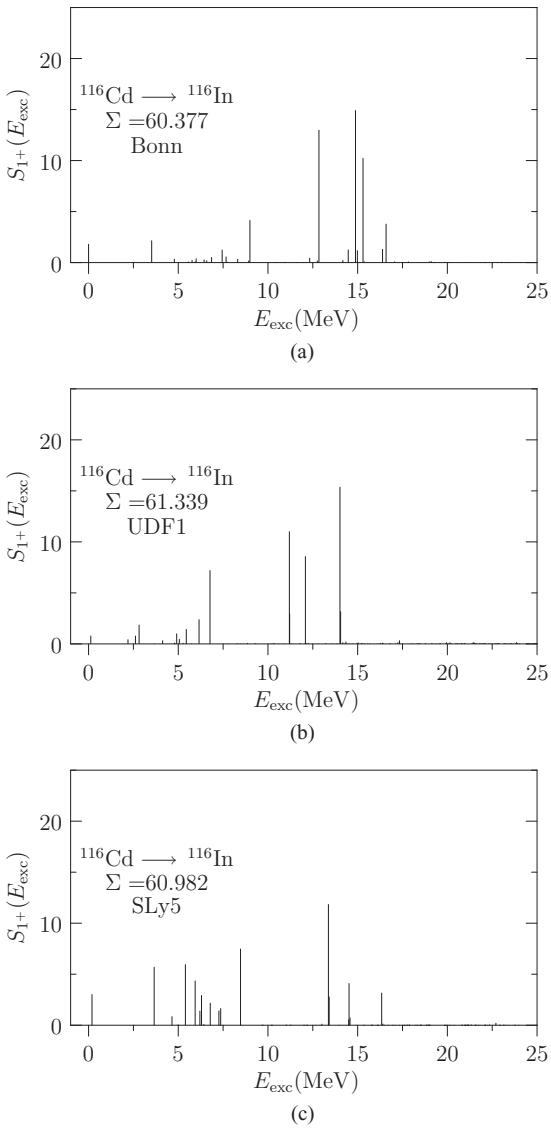

FIG. 2. The β^- strength for Gamow-Teller transitions to states computed by the Bonn one-boson-exchange potential (a) and different Skyrme interactions (b) and (c). The energies are normalized relative to the computed ground state of ^{116}In.

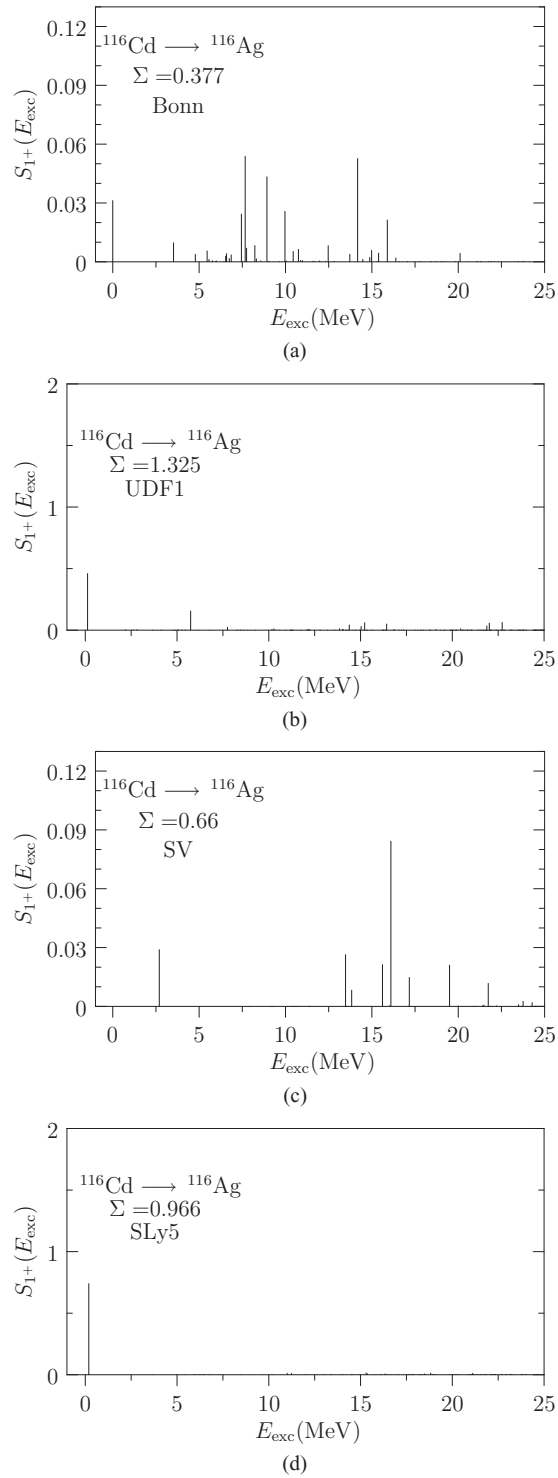

FIG. 3. The β^+ strength for Gamow-Teller transitions to states computed by the Bonn one-boson-exchange potential (a) and different Skyrme interactions (b–d). The energies are normalized relative to the computed ground state of ^{116}Ag.

TABLE IV. The GT transition strength to the first 1^+ state, 1^+_1, and the total GT strength to 1^+ states in ^{116}Ag computed by the Bonn and Skyrme interactions.

Interaction	Bonn	SkX	SkM*	SkP	SIII	SV
1^+_1 strength	0.031	0.46–0.55	0.94–1.04	1.33–1.44	0.20–0.28	0.027–0.031
Σ strength	0.377	0.777–0.872	1.473–1.585	1.538–1.651	0.958–1.045	0.658–0.662

UDF0	UDF1	SLy5	SLy4	SLy4d
0.73–0.79	0.43–0.48	0.71–0.77	0.30–0.33	0.18–0.20
1.245–1.318	1.30–1.35	0.93–1.001	0.836–0.859	0.746–0.766

by the other multipoles both vector and axial-vector kind of transitions may contribute at the same time.

For small momentum transfers, q, the cross sections are typically dominated by Gamow-Teller-like transitions mediated by the operator $F^{\mathrm{A}}(q)j_0(qr)\boldsymbol{\sigma}$ and Fermi-like ones which proceed via the operator $F^{\mathrm{V}}(q)j_0(qr)\mathbf{1}$. Additionally, for supernova neutrinos spin-dipole-like transitions of the form $F^{\mathrm{A}}(q)[j_1(qr)\boldsymbol{\sigma}\boldsymbol{Y}_1]_{0^-,1^-,2^-}$ turn out to be important. Here $F^{\mathrm{A}}(q)$ ($F^{\mathrm{V}}(q)$) is the axial-vector (vector) form factor; see, e.g., [9]. We have assumed the dipole form of these form factors with the quenched static value $F^A(0) = -1.00$.

IV. RESULTS

A. Parameters of the calculations

We compute the cross sections of the neutrino-nucleus and antineutrino-nucleus scatterings off ^{116}Cd in the charged-current channels. In our previous calculations [12] the required nuclear wave functions for the initial and final nuclear states were constructed using the quasiparticle random-phase approximation in its charge-changing mode (pnQRPA) where the mean field was of Woods-Saxon type and the two-body interaction was based on a G matrix of the Bonn one-boson-exchange type. In these new calculations the mean field is computed in a self-consistent way and the two-body interaction is of the Skyrme type. In our work we use a range of different values for the pairing strength G_1. The adjustments of this parameter have been made in such a way that the energy of the lowest proton-quasiparticle or neutron-quasiparticle state was roughly equal to the empirical gap $\Delta_{\mathrm{p}} = 1.437$ MeV for protons and $\Delta_{\mathrm{n}} = 1.371$ MeV for neutrons, determined from experimental masses by using the three-point formula [23]. Both empirical pairing gaps could not be reproduced simultaneously by a single value of G_1, so that we adopted a range of the pairing parameter values shown in Table I such that either the proton or neutron gap was reproduced as limiting cases. As stated earlier we use $G_0 \approx G_1$. To see how far we are from the breaking point of the pnQRPA we show in the third column of Table I the corresponding critical values of G_0 for which the breakdown occurs. This critical value is given as the ratio of the critical value to the value of G_1 for the two extreme values of G_1 indicated in column 2 of Table I. As can be seen the breakdown point is very far from the physical range of our present calculations and thus our results are robust against breakdown effects. In the same table we show also the magnitudes of the proton $Z = 50$ energy gap for each interaction, as well as the spin-parity (J^π) of the computed ground state of the odd-odd nucleus and the excitation energy of the first 1^+ state, 1^+_1. The ranges in $E(1^+_1)$ stem from the ranges of G_1 shown in column 2 of the table. From this table we observe that there are three groups of Skyrme interactions. The first group is formed by SkX, SkM*, SkP, UDF0, and UDF1 that need a relatively low pairing strength to overcome the single-particle energy gap at $Z = 50$. Quite the contrary concerns the SV interaction which has a large $Z = 50$ gap and thus a very big pairing strength is required. The third group is formed by SIII and the Lyon forces that have pairing strengths that fall between those of the previously mentioned groups. At this point it should be noted that in the present calculations the UDF forces are used without their own density dependent delta-pairing forces. These different pairing properties of the Skyrme forces correlate strongly with the different spin-isospin Gamow-Teller properties, as discussed below.

B. Gamow-Teller strength distributions and the IAS

Let us first discuss the β^- GT strength of transitions to the 1^+ states in ^{116}In. In all calculations we use here the effective quenched value $F^A(0) = -1.00$ for the axial-vector form factor. The energy centroids of the two satellites of the Gamow-Teller giant resonance (GTGR) in the Bonn calculation and in the Skyrme calculations are presented in Table II. The ranges of values of the energy centroids for the Skyrme interactions come from the ranges of value $G_0 = G_1$ in Table I. It is clear from Table II that the experimental

TABLE V. Empirical and calculated positions of the isobaric analog state (IAS) in ^{116}In. The energies are given relative to the ground state of ^{116}In.

Interaction	Empirical	Bonn	SkX	SkM*	SkP	SIII
Position of IAS (MeV)	12.04 [26]	12.06	12.37–12.91	10.95–11.68	11.28–11.98	12.16–12.87

UDF0	UDF1	SV	SLy5	SLy4	SLy4d
11.91–12.36	12.38–12.82	11.13–11.29	11.83–12.16	12.24–12.40	12.66–12.82

TABLE VI. Total cross sections for the charged-current neutrino scatterings off ^{116}Cd in units of 10^{-42}cm^2 as functions of the energy $E_{\mathbf{k}}$ of the incoming neutrino. The numbers in parenthesis refer to exponents. The last column of the table summarizes the full range of cross sections produced by all the Skyrme calculations quoted in the other columns of the table.

$E_{\mathbf{k}}$(MeV)	$(\sigma(E_{\mathbf{k}})^{\nu_e})_{\text{Bonn}}$	$(\sigma(E_{\mathbf{k}})^{\nu_e})_{\text{SkX}}$	$(\sigma(E_{\mathbf{k}})^{\nu_e})_{\text{SkM*}}$	$(\sigma(E_{\mathbf{k}})^{\nu_e})_{\text{SkP}}$
5.0	3.25 (0)	(2.64–2.97) (0)	(1.42–1.62) (0)	(4.26–5.90) (0)
10.0	2.02 (1)	(2.73–3.24) (1)	(1.00–1.29) (1)	(5.43–6.63) (1)
15.0	7.80 (1)	(1.28–1.45) (2)	(5.83–7.02) (1)	(2.06–2.36) (2)
20.0	2.65 (2)	(3.67–4.00) (2)	(2.02–2.36) (2)	(5.01–5.49) (2)
25.0	6.06 (2)	(7.15–7.60) (2)	(4.80–5.33) (2)	(8.79–9.39) (2)
30.0	1.07 (3)	(1.11–1.15) (3)	(8.46–9.09) (2)	(1.29–1.35) (3)
40.0	2.17 (3)	(2.04–2.10) (3)	(1.70–1.78) (3)	(2.33–2.42) (3)
50.0	3.72 (3)	(3.41–3.49) (3)	(2.88–2.98) (3)	(3.85–3.96) (3)
60.0	5.63 (3)	(5.20–5.31) (3)	(4.43–4.55) (3)	(5.88–6.02) (3)
70.0	7.89 (3)	(7.43–7.54) (3)	(6.31–6.45) (3)	(8.37–8.53) (3)
80.0	1.04 (4)	(1.00–1.01) (4)	(8.49–8.66) (3)	(1.13–1.14) (4)
$E_{\mathbf{k}}$(MeV)	$(\sigma(E_{\mathbf{k}})^{\nu_e})_{\text{UDF0}}$	$(\sigma(E_{\mathbf{k}})^{\nu_e})_{\text{UDF1}}$	$(\sigma(E_{\mathbf{k}})^{\nu_e})_{\text{SIII}}$	$(\sigma(E_{\mathbf{k}})^{\nu_e})_{\text{SV}}$
5.0	(1.89–2.16) (0)	(2.22–2.56) (0)	(1.57–1.69) (0)	(0.50–0.53) (0)
10.0	(2.24–2.57) (1)	(2.52–2.84) (1)	(9.07–11.0) (0)	(4.84–5.00) (0)
15.0	(1.02–1.14) (2)	(1.07–1.18) (2)	(4.76–5.72) (1)	(2.27–2.39) (1)
20.0	(3.20–3.45) (2)	(3.22–3.45) (2)	(1.76–2.07) (2)	(1.02–1.06) (2)
25.0	(6.57–6.92) (2)	(6.50–6.85) (2)	(4.41–4.91) (2)	(2.56–2.63) (2)
30.0	(1.06–1.10) (3)	(1.04–1.08) (3)	(7.91–8.52) (2)	(4.96–5.06) (2)
40.0	(2.03–2.09) (3)	(1.99–2.04) (3)	(1.58–1.66) (3)	(1.08–1.10) (3)
50.0	(3.39–3.46) (3)	(3.35–3.42) (3)	(2.70–2.80) (3)	(1.85–1.86) (3)
60.0	(5.19–5.28) (3)	(5.14–5.23) (3)	(4.17–4.30) (3)	(2.90–2.92) (3)
70.0	(7.38–7.48) (3)	(7.37–7.46) (3)	(6.00–6.14) (3)	(4.14–4.16) (3)
80.0	(9.91–10.02) (3)	(9.98–10.08) (3)	(8.10–8.26) (3)	(5.58–5.61) (3)
$E_{\mathbf{k}}$ (MeV)	$(\sigma(E_{\mathbf{k}})^{\nu_e})_{\text{SLy5}}$	$(\sigma(E_{\mathbf{k}})^{\nu_e})_{\text{SLy4}}$	$(\sigma(E_{\mathbf{k}})^{\nu_e})_{\text{SLy4d}}$	Full range
5.0	(5.04–5.53) (0)	(1.80–1.84) (0)	(1.57–1.60) (0)	(1.42–5.90) (0)
10.0	(5.10–5.60) (1)	(1.17–1.22) (1)	(1.01–1.04) (1)	(0.91–6.63) (1)
15.0	(1.88–1.99) (2)	(5.85–6.05) (1)	(5.25–5.45) (1)	(0.48–2.36) (2)
20.0	(4.48–4.69) (2)	(2.02–2.09) (2)	(1.77–1.84) (2)	(1.76–5.49) (2)
25.0	(7.84–8.08) (2)	(4.74–4.84) (2)	(4.31–4.42) (2)	(4.31–9.39) (2)
30.0	(1.15–1.18) (3)	(8.20–8.33) (2)	(7.65–7.79) (2)	(0.77–1.35) (3)
40.0	(2.06–2.10) (3)	(1.62–1.64) (3)	(1.54–1.56) (3)	(1.54–2.42) (3)
50.0	(3.47–3.52) (3)	(2.76–2.78) (3)	(2.63–2.66) (3)	(2.63–3.96) (3)
60.0	(5.31–5.38) (3)	(4.23–4.26) (3)	(4.06–4.09) (3)	(4.06–6.02) (3)
70.0	(7.60–7.67) (3)	(6.03–6.06) (3)	(5.81–5.85) (3)	(5.81–8.53) (3)
80.0	(1.02–1.03) (4)	(8.08–8.11) (3)	(7.80–7.84) (3)	(0.78–1.14) (4)

position of the major satellite of the GTGR at 14.5 MeV [24] can be reproduced using the Bonn interaction while none of the Skyrme interactions can achieve that. The minor satellite at 8.9 MeV [24] is only roughly reproduced by the Bonn potential while the SkM*, SIII, SLy4, and SLy4d do a better job. In fact, overall the SIII and SLy4 interactions do a rather nice job in reproducing the positions of the satellites of the GTGR. Also a general observation can be made based on Tables I and II: The pairing and Gamow-Teller properties of the Skyrme interactions correlate strongly. The SV interaction has a large energy gap at $Z = 50$ and thus a low single-particle level density at the proton Fermi surface which leads to much too high energies of the centroids of the two satellites of the giant resonance. On the other hand the single-particle $Z = 50$ energy gap is small for SkX, SkP, UDF0, and UDF1 so that the centroids are too low as compared with the data. For the rest of the forces, SkM*, SIII, SLy5, SLy4, and SLy4d, the level density seems to be reasonable since these forces reproduce reasonably the Gamow-Teller properties at the giant resonance region. All in all, the size of the $Z = 50$ gap in Table I correlates strongly with the energies of the satellites of the GTGR in Table II.

The sums of the measured [24] and computed Gamow-Teller strengths for the two satellites are shown in Table III where the ranges for the Skyrme interactions come from the ranges of G_1 in Table I. In the measurements performed in Ref. [24] only 60% of the total strength given by the Ikeda sum rule was observed. Therefore, the theoretical values of GTGR$_1$ in Table III have been multiplied by a factor of 0.6. In all Skyrme calculations the sum of the GT strength is outside the measured interval for GTGR$_2$ while the Bonn interaction does a nice job here. For GTGR$_1$ the sum of the GT strength is inside the measured interval for all interactions except for SkP, SLy5, and SV. The last line of Table III gives the GT

TABLE VII. The Same as Table VI for the charged-current antineutrino scatterings off ^{116}Cd.

$E_{\mathbf{k}}$ (MeV)	$(\sigma(E_{\mathbf{k}})^{\bar{\nu}_e})_{\text{Bonn}}$	$(\sigma(E_{\mathbf{k}})^{\bar{\nu}_e})_{\text{SkX}}$	$(\sigma(E_{\mathbf{k}})^{\bar{\nu}_e})_{\text{SkM*}}$	$(\sigma(E_{\mathbf{k}})^{\bar{\nu}_e})_{\text{SkP}}$
5.0				
10.0	1.12 (−2)	(3.36–4.06) (−2)	(7.01–7.84) (−2)	(9.67–10.6) (−2)
15.0	2.17 (−1)	(3.78–4.18) (−1)	(5.34–5.79) (−1)	(7.09–7.60) (−1)
20.0	1.05 (0)	(1.61–1.71) (0)	(1.72–1.83) (0)	(2.37–2.50) (0)
25.0	3.15 (0)	(4.50–4.67) (0)	(4.42–4.62) (0)	(5.92–6.16) (0)
30.0	7.13 (0)	(9.72–9.97) (0)	(9.20–9.50) (0)	(1.22–1.25) (1)
40.0	2.33 (1)	(2.99–3.03) (1)	(2.74–2.80) (1)	(3.60–3.67) (1)
50.0	5.61 (1)	(7.20–7.30) (1)	(6.46–6.57) (1)	(8.59–8.73) (1)
60.0	1.22 (2)	(1.54–1.56) (2)	(1.37–1.39) (2)	(1.81–1.84) (2)
70.0	2.31 (2)	(2.92–2.95) (2)	(2.59–2.62) (2)	(3.43–3.47) (2)
80.0	3.96 (2)	(4.95–5.00) (2)	(4.39–4.44) (2)	(5.79–5.86) (2)
$E_{\mathbf{k}}$ (MeV)	$(\sigma(E_{\mathbf{k}})^{\bar{\nu}_e})_{\text{UDF0}}$	$(\sigma(E_{\mathbf{k}})^{\bar{\nu}_e})_{\text{UDF1}}$	$(\sigma(E_{\mathbf{k}})^{\bar{\nu}_e})_{\text{SIII}}$	$(\sigma(E_{\mathbf{k}})^{\bar{\nu}_e})_{\text{SV}}$
5.0				
10.0	(5.47–6.03) (−2)	(3.36–3.78) (−2)	(1.82–2.38) (−2)	(2.80–2.81) (−3)
15.0	(4.74–5.06) (−1)	(3.59–3.83) (−1)	(2.83–3.17) (−1)	(1.65–1.70) (−1)
20.0	(1.80–1.88) (0)	(1.52–1.59) (0)	(1.25–1.33) (0)	(8.84–8.95) (−1)
25.0	(4.67–4.82) (0)	(4.20–4.31) (0)	(3.73–3.88) (0)	(2.98–3.01) (0)
30.0	(9.66–9.89) (0)	(8.95–9.12) (0)	(8.31–8.54) (0)	(7.17–7.22) (0)
40.0	(2.86–2.90) (1)	(2.71–2.74) (1)	(2.59–2.63) (1)	(2.35–2.36) (1)
50.0	(6.84–6.92) (1)	(6.52–6.58) (1)	(6.19–6.28) (1)	(5.46–5.48) (1)
60.0	(1.46–1.47) (2)	(1.39–1.40) (2)	(1.33–1.34) (2)	(1.165–1.169) (2)
70.0	(2.77–2.80) (2)	(2.65–2.67) (2)	(2.49–2.52) (2)	(2.13–2.14) (2)
80.0	(4.72–4.75) (2)	(4.50–4.53) (2)	(4.22–4.26) (2)	(3.54–3.55) (2)
$E_{\mathbf{k}}$ (MeV)	$(\sigma(E_{\mathbf{k}})^{\bar{\nu}_e})_{\text{SLy5}}$	$(\sigma(E_{\mathbf{k}})^{\bar{\nu}_e})_{\text{SLy4}}$	$(\sigma(E_{\mathbf{k}})^{\bar{\nu}_e})_{\text{SLy4d}}$	Full range
5.0				
10.0	(4.47–6.03) (−2)	(2.52–2.66) (−2)	(1.82–1.96) (−2)	(1.12–10.6) (−2)
15.0	(5.38–5.68) (−1)	(3.18–3.29) (−1)	(2.93–3.01) (−1)	(2.17–7.60) (−1)
20.0	(1.94–2.01) (0)	(1.26–1.29) (0)	(1.21–1.23) (0)	(1.05–2.50) (0)
25.0	(5.22–5.35) (0)	(3.62–3.67) (0)	(3.56–3.59) (0)	(3.15–6.16) (0)
30.0	(1.12–1.14) (1)	(7.92–8.00) (0)	(7.85–7.90) (0)	(0.71–1.25) (1)
40.0	(3.43–3.46) (1)	(2.43–2.45) (1)	(2.42–2.43) (1)	(2.33–3.67) (1)
50.0	(8.19–8.27) (1)	(5.79–5.82) (1)	(5.77–5.79) (1)	(5.61–8.73) (1)
60.0	(1.73–1.74) (2)	(1.23–1.24) (2)	(1.22–1.23) (2)	(1.22–1.84) (2)
70.0	(3.24–3.26) (2)	(2.33–2.34) (2)	(2.30–2.31) (2)	(2.31–3.47) (2)
80.0	(5.45–5.48) (2)	(3.96–3.97) (2)	(3.90–3.91) (2)	(3.96–5.86) (2)

strength going to the ground state of ^{116}In. For the ground-state transition our computed strengths agree with the measured value [25] only for SkM*, UDF0, and UDF1 and the rest of the interactions give too large strengths for this transition. For all the interactions, including the Bonn interaction, the first 1^+ state is almost a pure proton-$0g_{9/2}$–neutron-$0g_{7/2}$ configuration and the differences in the 1^+ strength in Table III come from the subtle interplay of this dominant contribution with a large number of tiny contributions in the 1^+ wave function. To see why the SV interaction produces a high 1^+_1 excitation energy we have plotted in Fig. 1 the proton-$0g_{9/2}$ and the neutron-$0g_{7/2}$ quasiparticle energies, and their sum, for all the Skyrme interactions of this work. As can be seen in the figure the neutron quasiparticle energy is very high for the SV interaction. This comes from the fact that for the SV interaction the neutron-$0g_{7/2}$ orbital is some 4 MeV away from the neutron Fermi surface whereas for the rest of the interactions this single-particle orbital is only some 0.5–2.0 MeV away from the Fermi surface. For protons the $0g_{9/2}$ orbital carries the two holes, and thus the proton-quasiparticle energy is practically the same for all the Skyrme forces.

The total 1^+ strength is slightly bigger for the Skyrme interactions than for the Bonn interaction. Our computations by using the Skyrme interactions produce the ground-state parities and spins of the odd-odd ^{116}Ag and ^{116}In nuclei listed in the fourth column of Table I. Experimentally, 1^+ is the ground state of ^{116}In and for the Bonn interaction the $J^\pi = 1^+$ is indeed the ground state. As can be seen in the table a 4^+ state is the ground state for the Skyrme interactions,

TABLE VIII. Values of the parameters α and T, and the average neutrino energies for the two adopted sets [30].

	$(\alpha_{\nu_e}, T_{\nu_e}, \langle E_{\nu_e}\rangle)$	$(\alpha_{\bar{\nu}_e}, T_{\bar{\nu}_e}, \langle E_{\bar{\nu}_e}\rangle)$
(I)	(3.0, 2.88, 11.5)	(3.0, 3.41, 13.6)
(II)	(0.0, 3.65, 11.5)	(0.0, 4.32, 13.6)

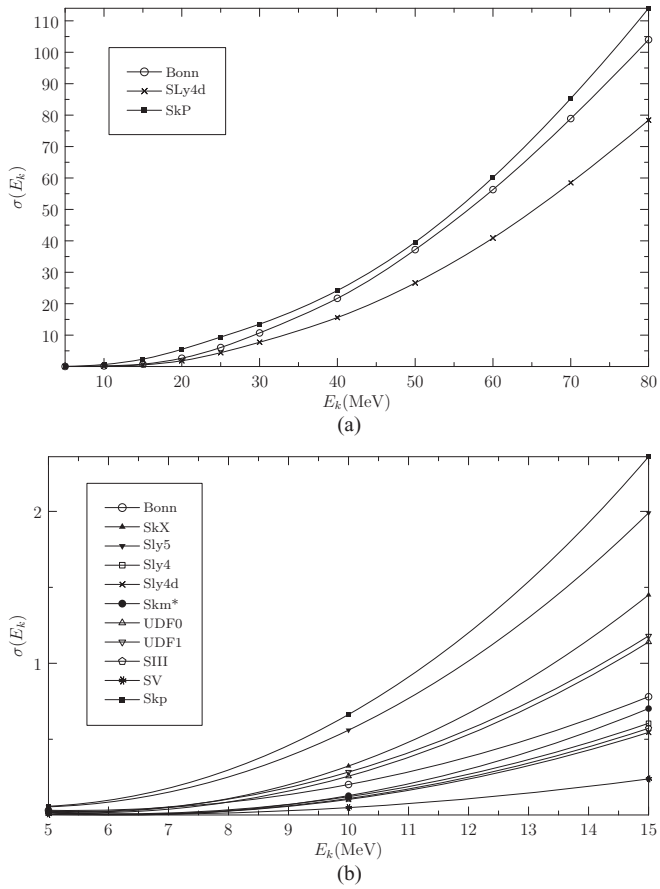

FIG. 4. The total cross sections for the Bonn and Skyrme calculations in units of 10^{-40} cm^2 as functions of the energy E_k of the incoming neutrino. The lower panel (b) shows the low-energy behavior of the cross sections and the upper panel (a) just the extreme Skyrme values plus the Bonn results for energies up to 80 MeV.

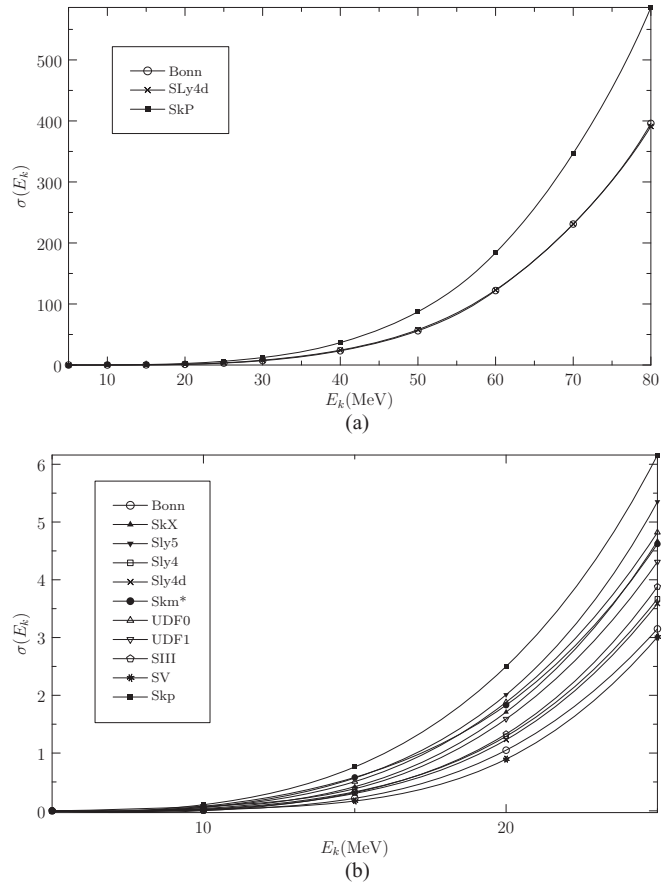

FIG. 5. The total cross sections for the Bonn and Skyrme calculations in units of 10^{-42} cm^2 as functions of the energy E_k of the incoming antineutrino. The lower panel (b) shows the low-energy behavior of the cross sections and the upper panel (a) just the extreme Skyrme values plus the Bonn results for energies up to 80 MeV.

except in the case of UDF1 for which 3^+ is the ground state. The large excitation energy for the SV interaction 2.7 MeV, is explained by the large two-quasiparticle energy of the proton-$0g_{9/2}$–neutron-$0g_{7/2}$ configuration as discussed above in the context of Fig. 1. It is clear from Tables II and III that the energy centroids and the sums of the GT strengths for the SV interaction are totally wrong, as also the first 1^+ state shoots sky-high. For all the interactions the states belonging to the major satellite of the giant resonance consist mainly of configurations proton-$0g_{7/2}$–neutron-$0g_{9/2}$, proton-$0h_{9/2}$–neutron-$0h_{11/2}$, and proton-$0h_{11/2}$–neutron-$0h_{9/2}$. For the states belonging to the minor satellite the configuration proton-$1d_{3/2}$–neutron-$1d_{5/2}$ plays a prominent role, with a sizable contribution coming from the proton-$0g_{7/2}$–neutron-$0g_{9/2}$ configuration. It is the subtle interplay between the $0g$-based configurations in the two satellites that distributes the Gamow-Teller strength between the satellites and produces the strongly varying patterns of distributions displayed in Table III.

Figures 2 and 3 compare the results of our calculations for the beta-decay strength of Gamow-Teller transitions to 1^+ states in ^{116}In and ^{116}Ag respectively, where the values of the pairing strength $G_0 = G_1$ used in the calculation presented in these figures are roughly in the middle of the ranges of Table I. In Fig. 2 we present three examples of the β^- strength distributions in ^{116}In. The strength distributions of the Bonn and UDF1 interaction look rather similar whereas the strength distribution obtained by the SLy5 interaction looks rather different, concentrating more on the low-energy side. As seen in Table III for SLy5 the strength of transition to the first 1^+ state is largely overestimated, for the Bonn interaction less so, and for UDF1 the strength is correctly reproduced. The Bonn and SLy5 interactions reproduce well the location of the major satellite (see Table II) but too much of the strength is shifted to lower energies for SLy5 (see Table III) which can be seen in the gross overestimation of the strength and underestimation of the energy of the centroid of the minor satellite (see Tables II and III). For UDF1 the locations of the centroids of the two GTGR satellites are shifted too low (see Table II) but the strength in the major satellite is correctly predicted whereas the strength in the minor satellite is too big, as is generally the case for all the Skyrme interactions (see Table III). In fact, only for the Bonn interaction the computed strength of the minor satellite comes close to the experimental value.

TABLE IX. Averaged cross sections for the charged-current neutrino-nucleus scattering off ^{116}Cd in units of 10^{-41} cm^2 as calculated for the two sets of neutrino parameters [(I) and (II)] of Table VIII. The last column of the table summarizes the full range of cross sections produced by all the Skyrme calculations quoted in the other columns of the table.

Parameters set	$(\nu_e)_{\text{Bonn}}$	$(\nu_e)_{\text{SkX}}$	$(\nu_e)_{\text{SkM*}}$	$(\nu_e)_{\text{SkP}}$
(I)	7.45	10.08–11.15	5.48–6.37	14.83–16.70
(II)	10.06	12.63–13.77	7.56–8.57	17.54–19.48
Parameters set	$(\nu_e)_{\text{UDF0}}$	$(\nu_e)_{\text{UDF1}}$	$(\nu_e)_{\text{SIII}}$	$(\nu_e)_{\text{SV}}$
(I)	8.68–9.43	8.88–9.61	4.83–5.58	2.68–2.77
(II)	11.18–12.01	11.32–12.12	6.79–7.66	3.95–4.07
Parameters set	$(\nu_e)_{\text{SLy5}}$	$(\nu_e)_{\text{SLy4}}$	$(\nu_e)_{\text{SLy4d}}$	Full range
(I)	13.50–14.24	5.51–5.68	4.94–5.09	4.83–16.70
(II)	15.89–16.65	7.56–7.75	6.82–7.01	6.79–19.48

In Fig. 3 we show four representative cases of the β^+ GT strength distributions. For the Bonn interaction the strength is rather uniformly distributed between 0 and 16 MeV whereas for UDF1 and SLy5 the strength lies in a single state, namely the ground state. For the SV interaction a group of states around 15 MeV is strongly populated (note that the scale of the figures for the Bonn and SV interactions is the same whereas for UDF1 and SLy5 the scale is much larger). For the Bonn interaction the transition strength to the ground state of ^{116}Ag is the same and more than one order of magnitude weaker than for the SLy5 and UDF1 interactions. Most likely the SLy5 and UDF1 interactions overestimate the ground-state strength. The same happens also for all the Skyrme interactions except for SV as shown in Table IV. According to this table the Bonn calculation predicts the smallest and the SkP calculation the largest total β^+ strength. The ranges in this table for the Skyrme interaction refer to the ranges of the pairing strength used in this work (see Sec. IV A). The transition strength to the 1^+ state for the SV interaction is similar to the Bonn interaction but the first 1^+ state of ^{116}Ag in the SV interaction is too high, about 2.6 MeV above the ground state (see Fig. 3).

In Table V we show the position of the isobaric analog state (IAS) in ^{116}In for the Bonn and Skyrme interactions and it is compared with the IAS position computed by using the empirical formula presented in Ref. [26]. For the Skyrme interactions the ranges of IAS energies are related to the ranges presented in Table I. In the Skyrme calculations the location of the IAS is well reproduced because the mean field and the residual interactions are treated self-consistently. In the Bonn calculation this is not the case since the single-particle energies and the residual Hamiltonian are produced separately. This inconsistency sets the energy of the IAS to 8.60 MeV in the Bonn calculation and leads to an unrealistically large 0^+ contribution to the neutrino-nucleus scattering cross section [12]. The problem can be circumvented by shifting manually the location of the IAS to its empirical position as done in the present calculations (see Table V).

At this point it is appropriate to mention that we tested the assumption of $G_0 \approx G_1$ by varying G_0 by 50% around the value $G_0 = G_1$ for typical Skyrme interactions. It turned out that the increase of the value of G_0 above the adopted value worsens the IAS and Gamow-Teller properties of the results, in particular making the GT feeding of the first 1^+ state in ^{116}In unphysically large. This was reflected in the neutrino and antineutrino scattering properties in such a way that the contribution from the first 1^+ dominated the scattering cross sections in an unphysical way. On the other hand, diminishing the value of G_0 below the adopted value brought no drastic changes to the IAS and GT properties of the calculations. The values of some observables improved, and some worsened relative to their experimental values. Thus it can be concluded that the choice $G_0 = G_1$ is a reasonable choice of the parameter values as pointed out in Ref. [19].

Finally, it should be stated that the nucleus ^{116}Cd has a deformation of $\beta_2 = 0.1$–0.2 (see, e.g., Refs [27] and [28]).

TABLE X. The same as Table IX for the charged-current antineutrino-nucleus scattering off ^{116}Cd.

Parameters set	$(\bar{\nu}_e)_{\text{Bonn}}$	$(\bar{\nu}_e)_{\text{SkX}}$	$(\bar{\nu}_e)_{\text{SkM*}}$	$(\bar{\nu}_e)_{\text{SkP}}$
(I)	0.067	0.096–0.101	0.100–0.106	0.135–0.141
(II)	0.108	0.150–0.155	0.149–0.155	0.198–0.206
Parameters set	$(\bar{\nu}_e)_{\text{UDF0}}$	$(\bar{\nu}_e)_{\text{UDF1}}$	$(\bar{\nu}_e)_{\text{SIII}}$	$(\bar{\nu}_e)_{\text{SV}}$
(I)	0.103–0.107	0.090–0.093	0.078–0.082	0.062–0.0623
(II)	0.154–0.158	0.138–0.142	0.125–0.130	0.103–0.104
Parameters set	$(\bar{\nu}_e)_{\text{SLy5}}$	$(\bar{\nu}_e)_{\text{SLy4}}$	$(\bar{\nu}_e)_{\text{SLy4d}}$	Full range
(I)	0.115–0.119	0.077–0.079	0.075–0.076	0.067–0.141
(II)	0.177–0.181	0.122–0.123	0.119–0.120	0.108–0.206

TABLE XI. Contributions of the dominant multipole channels to the averaged cross sections (I) of the neutrino scattering off ^{116}Cd in units of 10^{-42} cm^2. V = vector and AV = axial vector.

Interaction	0^+(V)	1^-(AV)	1^+(AV)	2^-(AV)	2^+(AV)
Bonn	8.91	0.86	53.62	3.28	0.20
SkX	3.92	0.75	87.69	3.07	0.20
SkM*	6.12	0.46	44.09	2.18	0.19
SkP	5.48	1.09	130.57	4.08	0.29
UDF0	4.62	1.05	72.16	3.24	0.24
UDF1	3.96	0.90	74.90	3.01	0.27
SIII	4.10	0.34	40.19	1.89	0.15
SV	6.44	0.09	17.92	0.39	0.15
SLy5	4.86	0.55	117.10	2.86	0.28
SLy4	4.33	0.38	44.06	1.65	0.21
SLy4d	3.75	0.31	39.57	1.51	0.19

Furthermore, for the double-beta-decay partners ^{116}Sn and ^{116}Cd one has that $\Delta\beta_2 \approx 0.1$. Based on the discussion in Ref. [29], we therefore estimate that the difference in deformation between the initial and final states could lead to a suppression of the neutrino cross sections of the order of 20%. Consequently, this effect is rather small compared to the discrepancies between the results computed with the various Skyrme interactions which are considered in this work.

C. Neutrino and antineutrino scattering cross sections

In Tables VI and VII we present the total cross sections for the neutrino-nucleus and antineutrino-nucleus scatterings as functions of the energy E_k of the incoming particles. The ranges of values of the total cross sections for the Skyrme calculations come from the ranges of values of $G_0 = G_1$ as indicated in Sec. IV A. It is clear from these tables that the Skyrme calculations produce results that are close to those of the Bonn calculations for both the neutrino and antineutrino scatterings. The calculations for neutrino scattering using the SkX, SLy5, UDF0, and UDF1 interactions predict slightly larger total cross sections for the low-energy part of the neutrino energies [except for $(E_{\mathbf{k}}) = 5$ MeV] and smaller total cross sections for the high-energy part as compared with the calculation based on the Bonn interaction. The SLy4, SLy4d, SkM*, SIII, and SV interactions predict smaller total cross sections and the SkP interaction predicts larger total cross sections than the Bonn interaction for all values of the neutrino energy. In the case of the antineutrino scattering the results for the SV interaction show slightly smaller total cross sections whereas the other Skyrme interactions show larger total cross sections than the Bonn ones for all values of the antineutrino energy.

The last columns of Tables VI and VII summarize the results of all calculations, i.e., they give the full range of cross sections predicted by Bonn interaction and all Skyrme interactions except for the SV interaction which was excluded since this interaction did not reproduce the energy of the first 1^+ state of both ^{116}In and ^{116}Ag (see Sec. IV B). Thus the full ranges of Tables VI and VII represent a quite solid range within which the true cross sections should lie. The planned experiments can then safely use these intervals for estimating their sensitivities, albeit the spread of the intervals is pretty large. To illustrate the situation further we show in Figs. 4 and 5 the total cross sections for the neutrino and antineutrino scatterings off ^{116}Cd as functions of the energy $E_{\mathbf{k}}$ of the incoming particle. In these figures we plot the highest values of the ranges in Tables VI and VII for the Skyrme interactions. In Fig. 4 one clearly sees that the Bonn results are within the interval produced by all the

TABLE XII. Contributions of the dominant multipole channels to the averaged cross sections (I) of the antineutrino scattering off ^{116}Cd in units of 10^{-42} cm^2. V = vector and AV = axial vector.

Interaction	0^-(AV)	1^-(V)	1^-(AV)	1^+(AV)	2^-(AV)	2^+(AV)	3^+(AV)
Bonn	0.028	0.196	0.232	0.039	0.139	0.015	0.019
SkX	0.128	0.151	0.296	0.222	0.179	0.017	0.021
SkM*	0.097	0.168	0.234	0.404	0.143	0.015	0.020
SkP	0.116	0.152	0.345	0.600	0.205	0.021	0.025
UDF0	0.140	0.153	0.260	0.332	0.147	0.021	0.023
UDF1	0.132	0.144	0.261	0.218	0.158	0.018	0.022
SIII	0.110	0.164	0.253	0.097	0.160	0.013	0.019
SV	0.049	0.199	0.182	0.010	0.144	0.004	0.009
SLy5	0.082	0.169	0.349	0.315	0.233	0.014	0.021
SLy4	0.081	0.169	0.213	0.128	0.149	0.011	0.017
SLy4d	0.085	0.175	0.222	0.077	0.153	0.010	0.017

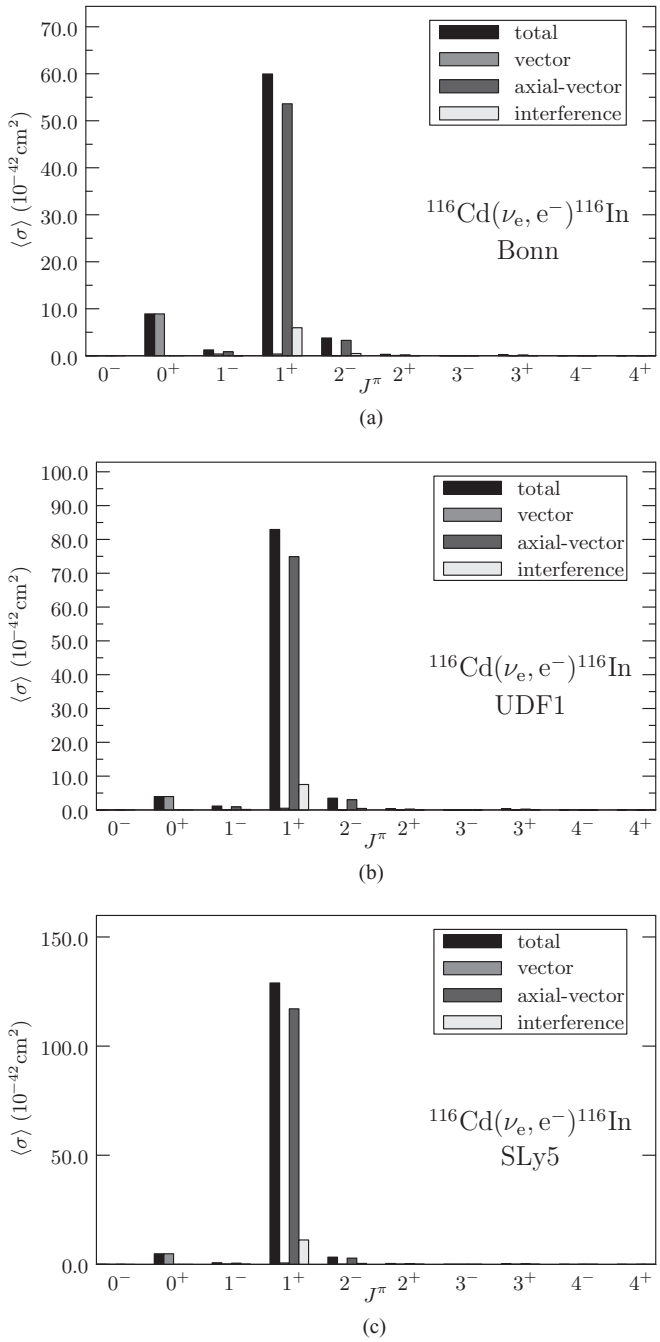

FIG. 6. Contributions of the dominant multipole channels to the averaged cross sections (I) of the neutrino scattering off ^{116}Cd for a selected set of interactions.

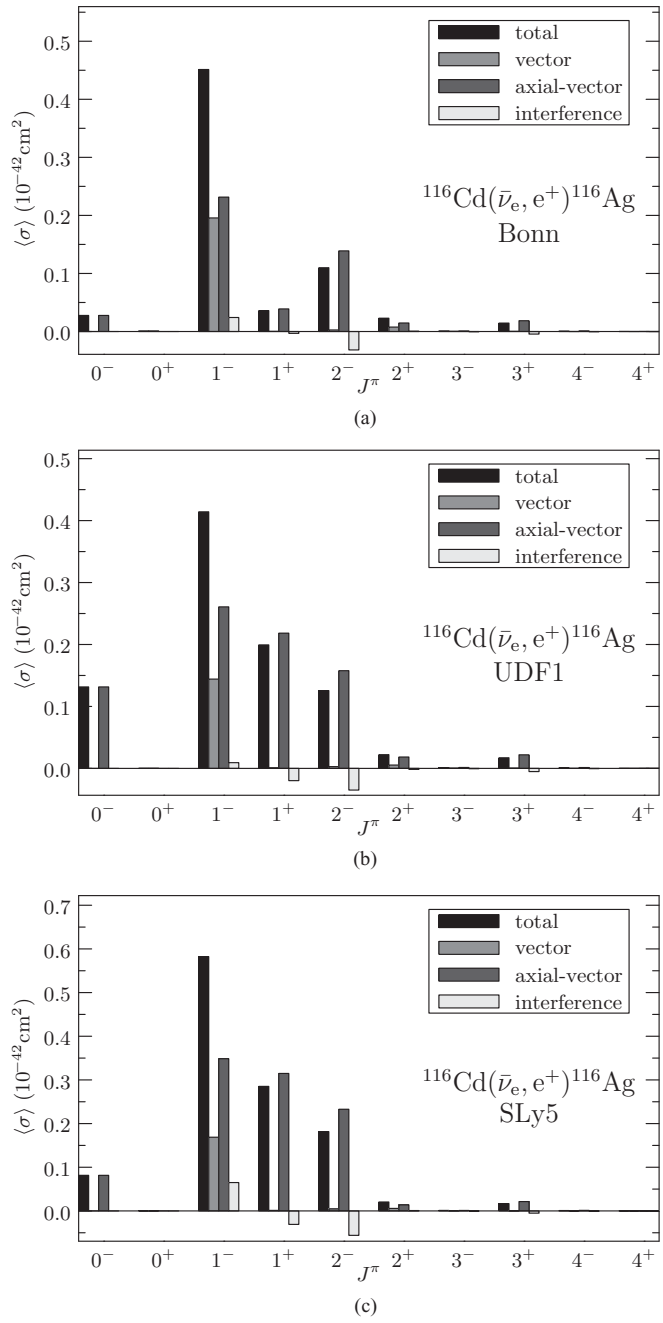

FIG. 7. Contributions of the dominant multipole channels to the averaged cross sections (I) of the antineutrino scattering off ^{116}Cd for a selected set of interactions.

Skyrme forces, even when just the top values of the intervals of the individual Skyrme calculation have been plotted. In Fig. 5, one can see that the Bonn interaction gives the lowest values of the antineutrino cross sections and the SLy4d interaction gives results close to the Bonn interaction. For reasons of clarity the plot of the cross sections has been divided to two parts: the low-energy one ($E_{\mathbf{k}} \leq 15$ MeV) and the higher-energy one ($E_{\mathbf{k}} \leq 80$ MeV). For the higher energies (upper panel) just the Bonn result and the two extreme cases of the Skyrme results have been plotted.

The averaged cross sections are obtained by folding the computed cross sections with the assumed Fermi-Dirac distribution of neutrino energies [10]. The energies of the neutrinos are described by a two-parameter distribution

$$F_{\mathrm{FD}}(E_{\mathbf{k}}) = \frac{1}{F_2(\alpha_\nu)T_\nu} \frac{(E_{\mathbf{k}}/T_\nu)^2}{1+\exp(E_{\mathbf{k}}/T_\nu - \alpha_\nu)}, \qquad (12)$$

where T_ν represents the effective neutrino temperature and α_ν is the so-called pinching parameter. In Eq. (12) the constant $F_2(\alpha_\nu)$ normalizes the total flux to unity. For a given value

TABLE XIII. The dominant transitions for the averaged cross section (I) in the reaction ^{116}Cd(ν_e,e^-)^{116}In. The triplet of numbers in the parentheses are first the spin-parity and ordinal (J^π_k), second the excitation energy in ^{116}In in units of MeV, and third the cross section in units of 10^{-41}cm^2.

Bonn	SkX	SkM*	SkP
(0^+_9, 12.06, 0.40)	(1^+_1, 0.24, 1.26)	(0^+_9, 11.33, 0.61)	(1^+_1, 0.04, 1.44)
(1^+_1, 0.0, 1.42)	(1^+_2, 3.53, 0.87)	(1^+_1, 0.07, 0.65)	(1^+_2, 2.52, 2.18)
(1^+_2, 3.52, 0.99)	(1^+_{11}, 5.96, 1.28)	(1^+_2, 3.72, 0.52)	(1^+_8, 4.75, 1.07)
(1^+_{21}, 8.99, 0.60)	(1^+_{13}, 7.35, 2.34)	(1^+_{10}, 6.90, 0.53)	(1^+_{10}, 5.03, 1.57)
(1^+_{36}, 12.84, 0.79)	(1^+_{29}, 11.12, 1.62)	(1^+_{16}, 9.10, 1.71)	(1^+_{13}, 6.49, 2.38)
(1^+_{40}, 14.88, 0.51)			(1^+_{24}, 10.63,1.68)
(1^+_{42}, 15.30, 0.31)			
UDF0	UDF1	SIII	SV
(1^+_1, 0.05, 0.65)	(1^+_1, 0.12, 0.59)	(0^+_{10}, 12.53, 0.41)	(0^+_5, 11.21, 0.62)
(1^+_2, 2.44, 0.66)	(1^+_4, 2.82, 0.93)	(1^+_1, 0.54, 0.89)	(1^+_1, 2.69, 0.69)
(1^+_6, 4.24, 0.59)	(1^+_{15}, 6.77, 1.82)	(1^+_2, 5.07, 0.31)	(1^+_2, 7.90, 0.35)
(1^+_{16}, 6.84, 2.72)	(1^+_{28}, 11.19, 0.99)	(1^+_{12}, 8.06, 0.60)	(1^+_{15}, 14.17, 0.46)
(1^+_{37}, 11.66, 1.64)	(1^+_{33}, 12.09, 0.61)	(1^+_{15}, 9.44, 0.49)	
	(1^+_{41}, 14.01, 0.65)	(1^+_{16}, 9.51, 0.59)	
		(1^+_{28}, 13.66, 0.40)	
		(1^+_{31}, 14.55, 0.33)	
		(1^+_{40}, 16.70, 0.42)	
SLy5	SLy4		SLy4d
(1^+_1, 0.19, 2.24)	(0^+_9, 12.33, 0.43)		(0^+_9, 12.74, 0.37)
(1^+_2, 3.66, 2.52)	(1^+_1, 0.28, 0.85)		(1^+_1, 0.64, 0.87)
(1^+_5, 5.40, 1.94)	(1^+_2, 3.82, 0.51)		(1^+_2, 4.41, 0.42)
(1^+_6, 5.94, 1.22)	(1^+_{10}, 7.07, 0.36)		(1^+_{10}, 7.20, 0.28)
(1^+_{13}, 8.47, 1.31)	(1^+_{13}, 9.42, 1.23)		(1^+_{12}, 8.27, 0.33)
	(1^+_{31}, 15.15, 0.54)		(1^+_{15}, 9.82, 1.38)
			(1^+_{31}, 15.60, 0.42)
			(1^+_{38}, 17.20, 0.37)

of α_ν the temperature T_ν can be computed from the average neutrino energy $\langle E_\nu \rangle$ by using the relation

$$\langle E_\nu \rangle / T_\nu = \frac{F_3(\alpha_\nu)}{F_2(\alpha_\nu)}, \tag{13}$$

where

$$F_k(\alpha_\nu) = \int \frac{x^k dx}{1 + \exp(x - \alpha_\nu)}. \tag{14}$$

The values of the parameters α and T and the corresponding average neutrino energies $\langle E_\nu \rangle$ used in this work are presented in Table VIII. The resulting averaged cross sections for the neutrino-nucleus and antineutrino-nucleus scatterings are shown in Tables IX and X respectively. In the Skyrme calculations the ranges of cross sections stems from the ranges of adopted values of $G_0 = G_1$ pairing parameters. The full ranges of cross sections computed by using all interactions are indicated in the last columns of the tables. It is clear from Table IX that the average neutrino cross sections are the largest for the interactions SkX, SkP, and SLy5 and the smallest for the interactions SkM*, SIII, SV, SLy4, and SLy4d. The results for UDF0 and UDF1 very much resemble those of the Bonn interaction. It is also clear that the results of Skyrme calculations span a wide range of cross-section values, the Bonn results being roughly in the middle. From Table X one notices that the averaged antineutrino cross sections in the Skyrme calculations are larger than in the Bonn calculation except for the SV interaction. It should be noted that here the SIII, SV, SLy4, and SLy4d interactions produce rather similar results as the Bonn interaction. Also the results of the UDF0 and UDF1 interactions are not far from the Bonn results, meaning that the results of these interactions behave similarly to the Bonn results for both the neutrino and antineutrino scatterings. The full range of the results for the $\bar{\nu}$ scattering is much narrower than the full range of the ν scattering results.

We display in Tables XI and XII the contributions of the dominant multipoles to the cross sections for both the neutrino and antineutrino scatterings. In these tables we present the result for the pairing strength $G_0 = G_1$ which are in the middle of the ranges of Table I. The multipole contributions have been computed for the averaged cross sections with the parameters (I) of Table VIII. In Figs. 6 and 7 we illustrate these contributions for the Bonn, UDF1, and SLy5 interactions that were also used in the β^+ and β^- strength analyses of Figs. 2 and 3. These figures show also separately the contributions to each multipole from axial-vector, vector, and interference components of the nuclear current. By looking at Tables XI and XII it can be concluded that for the neutrino scattering the contributions from the 1^+ multipole are the most significant in the Skyrme calculations as also in the Bonn calculation. Except for the 0^+

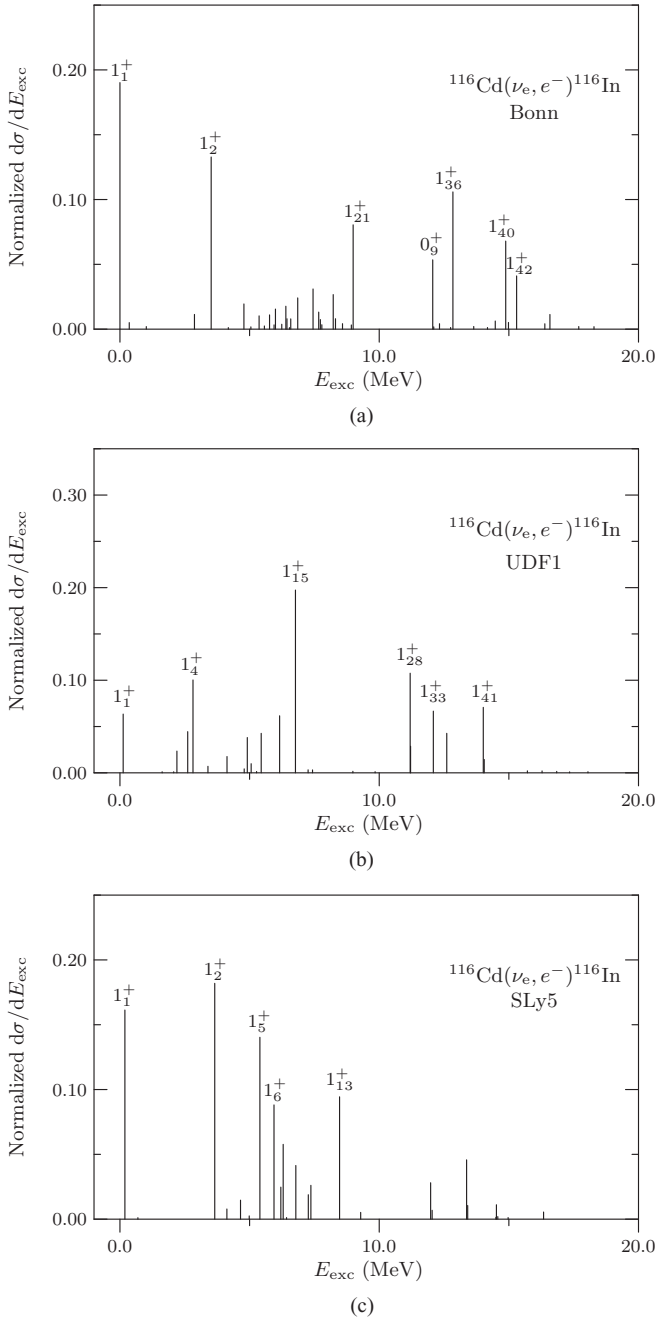

FIG. 8. Normalized averaged (I) differential cross sections as functions of the excitation energy in ^{116}In for the neutrino scattering off ^{116}Cd calculated for three representative interactions. The sum of contributions in each panel is 1.

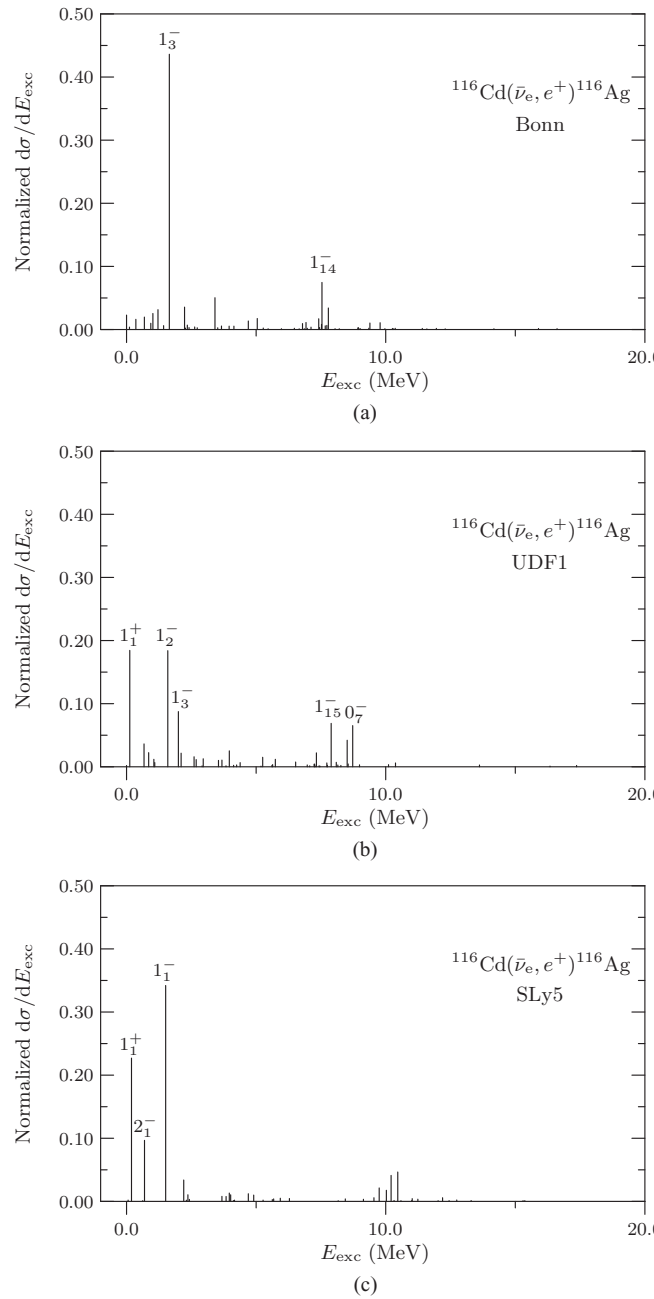

FIG. 9. Normalized averaged (I) differential cross sections as functions of the excitation energy in ^{116}Ag for the antineutrino scattering of ^{116}Cd calculated for three representative interactions. The sum of contributions in each panel is 1.

contribution the Bonn results are similar to the Skyrme results. For the antineutrino scattering we can see that the contributions from the 0^- and 1^+ multipoles become more effective in the Skyrme calculations, except for the SV interaction for which the contribution from 1^+ is less than for the Bonn interaction. For the other multipoles the Bonn results behave in the same way as those of the Skyrme calculations. It is also noteworthy that even though the β^- strength distributions produced by the UDF1 and SLy5 calculations (Fig. 2) are quite different the multipole contributions to the neutrino-nucleus cross sections are relatively similar for both interactions.

From Fig. 7 one perceives the small 0^- contribution to the multipole decomposition of the antineutrino-nucleus cross section for the Bonn calculation. The 1^- and 2^- contributions are roughly the same in the Bonn and Skyrme calculations whereas for the 1^+ multipole the contribution in the Bonn calculation is much weaker than in the Skyrme calculations. Contrasting with the β^+ strength distributions of Fig. 3 where the UDF1 and SLy5 interactions gave essentially one

TABLE XIV. The dominant transitions for the averaged cross section (I) in the reaction ^{116}Cd($\bar{\nu}_e$,e^+)^{116}Ag. The triplet of numbers in the parentheses are first the spin-parity and ordinal (J^π_k), second the excitation energy in ^{116}Ag in units of MeV, and third the cross section in units of 10^{-43}cm^2.

Bonn	SkX	SkM*	SkP
(1^-_3, 1.65, 2.90)	(0^-_6, 8.67, 0.94)	(1^+_1, 0.07, 3.59)	(1^+_1, 0.04, 5.11)
(1^-_{14}, 7.54, 0.50)	(1^+_1, 0.24, 1.80)	(1^-_1, 1.15, 2.18)	(1^-_1, 1.60, 2.79)
	(1^-_2, 1.46, 0.85)		
	(1^-_3, 1.85, 2.03)		
	(1^-_{15}, 8.07, 0.73)		
	(2^-_1, 0.74, 0.66)		
UDF0	UDF1	SIII	SV
(0^-_7, 8.38, 1.06)	(0^-_7, 8.73, 0.60)	(0^-_6, 10.03, 0.62)	(1^-_1, 2.10, 3.38)
(1^+_1, 0.05, 2.80)	(1^+_1, 0.12, 1.68)	(1^+_1, 0.54, 0.80)	(2^-_1, 2.15, 0.71)
(1^-_3, 1.63, 1.50)	(1^-_2, 1.59, 1.68)	(1^-_2, 1.20, 1.39)	(1^-_9, 11.95, 0.38)
	(1^-_3, 2.00, 0.80)	(1^-_3, 1.59, 1.51)	
	(1^-_{15}, 7.90, 0.63)	(2^-_1, 0.57, 0.52)	
SLy5	SLy4		SLy4d
(1^+_1, 0.19, 2.66)	(0^-_6, 10.72, 0.51)		(0^-_6, 10.76, 0.53)
(1^-_1, 1.51, 4.00)	(1^+_1, 0.28, 1.10)		(1^+_1, 0.64, 0.63)
(2^-_1, 0.69, 1.13)	(1^-_1, 1.64, 2.48)		(1^-_1, 1.31, 1.91)
	(1^-_2, 2.10, 0.69)		(1^-_2, 1.69, 1.29)
	(1^-_{14}, 9.92, 0.43)		(2^-_1, 0.68, 0.59)
	(2^-_1, 0.91, 0.61)		

contribution (a strong ground-state strength) and the Bonn interaction a widely spread distribution, one can conclude that the large contribution of the 1^+ multipole in the Skyrme calculations is unrealistic and stems from the overly large strength to the ground state of ^{116}Ag. The same flaw plagues practically all the present Skyrme calculations as seen in Table XII.

The averaged differential cross sections for the Bonn, UDF0 and SLy5 interactions of the reactions ^{116}Cd(ν_e,e^-)^{116}In and ^{116}Cd($\bar{\nu}_e$,e^+)^{116}Ag as functions of the excitation energy in the final nuclei are presented in Figs. 8 and 9 respectively. The cross sections have been normalized by dividing by the total averaged cross section $\langle\sigma\rangle$, i.e., the sums of all contributions in the figures are 1. In Tables XIII and XIV we illustrate the most prominent final states, their excitation energies and their strength for all interactions. In these tables as well as in Figs. 8 and 9 we show the results for values of $G_0 = G_1$ which are roughly in the middle of the ranges given in Table I. The prominent final states for the reaction ^{116}Cd(ν_e,e^-)^{116}In are 1^+ for all interactions. There are also contributions from excitations to one prominent 0^+ state for the Bonn, SkM*, SIII, SV, SLy4, and SLy4d interactions, which is the IAS. The contributions from the first 1^+ state, 1^+_1, range from 0.59 (UDF1) to 2.24 (SLy5). The Bonn calculation gives 1.42. In fact, there is a strong correlation between the sizes of the 1^+_1 contributions of Table XIII and the strengths of the Gamow-Teller transitions to the 1^+_1 state in ^{116}In, displayed in Table III. This correlation remains up to rather high energies of the impinging neutrino. From Fig. 8 one observes that the general pattern of the dominating 1^+ contributions is similar for the Bonn and UDF1 interactions, the SLy5 interaction producing a totally different pattern. This is qualitatively in line with the similar/different patterns of the Gamow-Teller β^- strength distributions displayed for the same interactions in Fig. 2.

As seen from Table XIV most of the prominent final states for the reaction ^{116}Cd($\bar{\nu}_e$,e^+)^{116}Ag are 1^- for all interactions. For the Skyrme interactions there is a strong contribution coming from the excitation to the first 1^+ state. Also a contribution from the transition to a 0^- state appears for the SkX, UDF0, UDF1, SIII, SLy4, and SLy4d interactions. A contribution coming from a 2^- state appears for the SkX, SIII, SV, SLy4, SLy4d and SLy5 interactions. The strong 1^+_1 contribution in the Skyrme calculations relates to the strong peak of the β^+ Gamow-Teller strength at zero energy, visible in the lower panels of Fig. 3. From Fig. 9 one observes that the cross-section pattern of the Bonn interaction is much closer to the one of the UDF1 interaction than the one of the SLy5 interaction. This observation together with the patterns of Figs. 2 and 8 imply that the properties of the Bonn interaction are closer to the properties of the UDF1 interaction than the properties of the SLy5 interaction. Comparing the broad range of results produced by the Bonn and Skyrme interactions, for all the presently discussed Gamow-Teller and neutrino-scattering observables, one could conclude that the UDF1 interaction is consistent with the Bonn interaction and in fact, overall, closest to it of all the Skyrme interactions. The SLy5 is maybe the farthest from the Bonn interaction judging by the results quoted in this work.

V. SUMMARY AND CONCLUSIONS

In this work we have studied the charged-current cross sections for neutrino and antineutrino scatterings off ^{116}Cd

using ten different Skyrme interactions. The cross sections have been calculated for neutrino energies which are appropriate for supernova neutrinos. The nuclear response of ^{116}Cd to supernova neutrinos and antineutrinos has been estimated by folding the computed cross sections with a two parameter Fermi-Dirac neutrino-energy distribution. The resulted cross sections has been compared with those computed by using a Bonn G-matrix interaction.

The computed β^- Gamow-Teller strength and the positions of the major and minor satellites of the Gamow-Teller giant resonance in ^{116}In have been compared with the experimental ones. We have found that the result corresponding to the Bonn interaction are more in agreement with the experimental results than the results corresponding to the Skyrme interactions.

Our results show that the neutrino and antineutrino scattering cross sections computed by using the Bonn interaction are within the interval produced by all the Skyrme interactions. In this way our calculations predict a range of cross sections within which the true cross sections should lie.

We have found that the neutrino cross sections are dominated by transition to 1^+ states for all Skyrme interactions as well as for the Bonn interaction. In the case of the Bonn, SkM*, SV, SIII, SLy4, and SLy4d interactions a significant contribution arises from the isobaric analog state. The antineutrino cross sections are dominated by transitions to 1^- states for all Skyrme interactions and also by a transition to the first 1^+ state, except for the SV interaction. Contributions from the 0^- and 2^- states appear for some Skyrme interactions.

Finally, based on the results of this work, we can say that the UDF1 is the closest of all Skyrme interactions to the Bonn interaction and the SLy5 is the farthest one when considering charge-changing processes in ^{116}Cd.

ACKNOWLEDGMENTS

This work was supported by the Academy of Finland under the Finnish Center of Excellence Program 2012–2017 (Nuclear and Accelerator Based Program at JYFL) and by the Academy of Finland and University of Jyväskylä within the FIDIPRO program.

[1] D. V. Forero, M. Tòrtola, and J. W. F. Valle, Phys. Rev. D **86**, 073012 (2012).
[2] M. Kuze, arXiv:1303.1289.
[3] J. Suhonen and O. Civitarese, Phys. Rep. **300**, 123 (1998).
[4] K. Zuber, Prog. Part. Nucl. Phys **57**, 235 (2006).
[5] H. Ejiri, Phys. Rep. **338**, 265 (2000).
[6] K. Scholberg, Annu. Rev. Nucl. Part. Sci. **62**, 81 (2012).
[7] C. Volpe, J. Phys. G: Nucl. Part. Phys. **31**, 903 (2005).
[8] M. Bender, P.-H. Heenen, and P.-G. Reinhard, Rev. Mod. Phys. **75**, 121 (2003).
[9] E. Ydrefors and J. Suhonen, Adv. High Energy Phys. **2012**, 373946 (2012).
[10] E. Ydrefors, K. G. Balasi, T. S. Kosmas, and J. Suhonen, Nucl. Phys. A **896**, 1 (2012).
[11] K. Holinde, Phys. Rep. **68**, 121 (1981).
[12] W. Almosly, E. Ydrefors, and J. Suhonen, J. Phys. G: Nucl. Part. Phys. **40**, 095201 (2013).
[13] M. Dutra, O. Lourenco, J. S. Sá Martins, A. Delfino, J. R. Stone, and P. D. Stevenson, Phys. Rev. C **85**, 035201 (2012).
[14] M. Kortelainen *et al.*, Phys. Rev. C **85**, 024304 (2012).
[15] B. G. Carlsson, J. Dobaczewski, J. Toivanen, and P. Vesely, Comput. Phys. Commun. **181**, 1641 (2010).
[16] B. G. Carlsson, J. Toivanen, J. Dobaczewski, P. Vesely, Y. Gao, and D. Ward (unpublished).
[17] P. Vesely, J. Toivanen, B. G. Carlsson, J. Dobaczewski, N. Michel, and A. Pastore, Phys. Rev. C **86**, 024303 (2012).
[18] B. G. Carlsson, J. Toivanen, and A. Pastore, Phys. Rev. C **86**, 014307 (2012).
[19] B. G. Carlsson and J. Toivanen (unpublished).
[20] J. D. Walecka, *Theoretical Nuclear and Subnuclear Physics* (Imperial College Press, London, 2004).
[21] J. S. O'Connell, T. W. Donnelly, and J. D. Walecka, Phys. Rev. C **6**, 719 (1972).
[22] E. Ydrefors, K. G. Balasi, J. Suhonen, and T. S. Kosmas, *Neutrinos: Properties, Reactions, Sources and Detection* (Nova Science, Hauppauge, NY, 2011).
[23] J. Suhonen, *From Nucleons to Nucleus: Concepts of Microscopic Nuclear Theory* (Springer, Berlin, 2007).
[24] H. Akimune *et al.*, Phys. Lett. B **394**, 23 (1997).
[25] C. Wrede *et al.*, Phys. Rev. C **87**, 031303(R) (2013).
[26] Y. Z. Qian, W. C. Haxton, K. Langanke, and P. Vogel, Phys. Rev. C **55**, 1532 (1997).
[27] P. Raghavan, At. Nucl. Data Tables **42**, 189 (1989).
[28] S. Raman, Ch. Malarkey, W. T. Milner, C. W. Nestor Jr., and P. H. Stelson, At. Nucl. Data Tables **36**, 1 (1987).
[29] J. Suhonen and O. Civitarese, Nucl. Phys. A **847**, 207 (2010).
[30] M. T. Keil and G. G. Raffelt, Astrophys. J. **590**, 971 (2003).